Kriging-Based Reliability Analysis Considering Predictive Uncertainty Reduction

Meng Li[1], Sheng Shen[1], Vahid Barzegar[2], Mohammadkazem Sadoughi[1], Simon Laflamme[2,3], and Chao Hu[1,3*]

[1] *Department of Mechanical Engineering, Iowa State University*
Ames, IA 50011 USA

[2] *Department of Civil, Construction, and Environmental Engineering, Iowa State University*
Ames, IA 50011 USA

[3] *Department of Electrical and Computer Engineering, Iowa State University*
Ames, IA 50011 USA

Abstract

Over the past decade, several acquisition functions have been proposed for sequential kriging-based reliability analysis. Each of these acquisition functions can be used to identify an optimal sequence of samples to be included in the kriging model. However, no single acquisition function provides better performance over the others in all cases. Further, the best-performing acquisition function can change at different iterations over the sequential sampling process. To address this problem, this paper proposes a new acquisition function, namely expected uncertainty reduction (EUR), that serves as a meta-criterion to select the best sample from a set of optimal samples, each identified from a large number of candidate samples according to the criterion of an acquisition function. EUR does not rely on the local utility measure derived based on the kriging posterior of a performance function as most existing acquisition functions do. Instead, EUR directly quantifies the expected reduction of the uncertainty in the prediction of limit-state function by adding an optimal sample. The uncertainty reduction is quantified by sampling over the kriging posterior. In the proposed EUR-based sequential sampling process, a portfolio that consists of four acquisition functions is first employed to suggest four optimal samples at each iteration of sequential sampling. Each of these samples is optimal with respect to the selection criterion of the corresponding acquisition function. Then, EUR is employed as the meta-criterion to identify the best sample among those optimal samples. The results from two mathematical and one practical case studies show that (1) EUR-based sequential sampling can perform as well as or outperform the single use of any acquisition function in the portfolio, and (2) the best-performing acquisition function may change from one problem to another or even from one iteration to the next within a problem.

Keywords: Sequential sampling, expected uncertainty reduction, reliability analysis, multiple acquisition functions

1 Introduction

Reliability is defined as the probability that an engineered system can meet the performance requirement under all sources of uncertainties [1,2]. To quantify the reliability of an engineered system, the input parameters are usually modeled as random variables that follow certain distributions. The reliability of this system is then expressed as a multi-dimensional integration of the joint probability density function (PDF) of these random variables [3]:

$$R = \int_{\Omega^S} f(\mathbf{x})\, d\mathbf{x} \tag{1}$$

where $\mathbf{x}$ denotes the random variables, $f(\mathbf{x})$ denotes the joint PDF of the random variables, and Ω^S denotes the safety region that is defined based on the sign of the performance function $G(\mathbf{x})$ as $\Omega^S = \{\mathbf{x}: G(\mathbf{x}) < 0\}$. The boundary $G(\mathbf{x}) = 0$ that separates the safety region and the failure region (i.e., $\Omega^F = \{\mathbf{x}: G(\mathbf{x}) \geq 0\}$) is named the limit-state function (LSF) [4]. To solve for the reliability in Eq. (1), the most commonly used method is Monte Carlo simulation (MCS) [4], which simulates the joint PDF $f(\mathbf{x})$ by generating a large number of random samples. The reliability level can then be approximated as the ratio of the number of random samples in the safety region to the total number of MCS samples (n_{MCS}). Generally, a large sample size (e.g., $n_{MCS} = 10^6$ or 10^7) is required to achieve an accurate reliability estimation with MCS. However, the large sample sizes may incur an extremely high computational cost when the evaluation of the performance function is computationally expensive [5].

To reduce the computational cost of the direct MCS, a popular approach is to approximate the computationally expensive performance function $G(\mathbf{x})$ with a computationally cheap surrogate model $\hat{G}(\mathbf{x})$, built with a small set of

* *E-mail addresses:* chaohu@iastate.edu; huchaostu@gmail.com (C. Hu).

sample data set [6]. A number of surrogate modeling methods have been proposed for reliability analysis, such as dimension reduction methods [7-9], stochastic spectral methods [10-12], and kriging (or Gaussian process)-based methods [3, 13-20]. Among these methods, kriging-based methods are unique because of their ability in constructing the surrogate models following a sequential manner. Thus, our review is mainly focused on the kriging-based methods.

Kriging is a probabilistic surrogate model that provides both the predicted value of a performance function and the uncertainty of this prediction [21]. Thanks to this property, kriging-based methods can build a surrogate model following a two-step process, in which an initial model is first constructed with an initial data set (e.g., samples generated by the Latin hypercube sampling (LHS) technique), and the model is then refined by sequentially and iteratively selecting new samples. The key to implementing this process is to define a proper acquisition function. At each iteration, the sample that maximizes the acquisition function is identified from a large pool of candidate sample points and this optimal sample is added to the sample data set [22]. In general, a high accuracy in the approximation of the LSF, which separates the safety and failure regions, leads to a high accuracy in reliability analysis. Therefore, an acquisition function should be defined in a way that high values of the acquisition function correspond to (i) regions close to the LSF (exploitation), (ii) regions with high uncertainty in the LSF prediction (exploration), or (iii) both.

Based on this principle, several acquisition functions have been proposed for sequential kriging-based reliability analysis. Among these acquisition functions, four representative ones are selected in this study and reviewed in Subsection 2.2: expected feasibility function (EFF) [15], maximum confidence enhancement (MCE) [16], expected risk function (ERF) [17], and sequential exploration-exploitation with dynamic trade-off (SEEDT) [18]. By comparing the four acquisition functions, we find that the main difference among the four acquisition functions is the shapes of their utility functions over the performance function (or output) space. The utility function in MCE takes the shape of the Heaviside step function, while those in EFF and ERF take triangle shapes. Unlike MCE, EFF, and ERF, SEEDT uses a utility function that takes the shape of a Gaussian decay function. Additionally, MCE, EFF, and ERF assume a fixed balance between exploration and exploitation, while SEEDT introduces an exploration-exploitation trade-off coefficient that adaptively weighs exploration and exploitation throughout sequential sampling process.

However, no single acquisition function provides better performance over others on all problem cases [23]. Even within one problem case, the best-performing acquisition function can change at various stages of the sequential sampling process. To address this issue, Shahriari et al. [24] proposed the use of a portfolio consisting of multiple acquisition functions for Bayesian optimization. At each iteration, a meta-criterion considering the information gain toward the optimum is used to select the best sample among the *optimal* samples suggested by the acquisition functions. This meta-criterion was proposed to tackle Bayesian optimization problems and cannot be directly adopted for reliability analysis. This is because the goal of sequential kriging-based reliability analysis is to provide satisfactory accuracy in approximating the LSF, rather than maximizing or minimizing the performance function (or response) as in Bayesian optimization. The objective of our study is to apply the portfolio of multiple acquisition functions to sequential kriging-based reliability analysis. To do so, we first define an uncertainty indicator of the LSF prediction, which indirectly measures the LSF prediction accuracy of the kriging model. Then, we propose a meta-criterion, namely expected uncertainty reduction or EUR, to select the best sample among the optimal samples suggested by the acquisition functions in the portfolio.

The reminder of this paper is organized as follows. Section 2 briefly reviews the kriging model and the four acquisition functions used in this study. Section 3 introduces the proposed EUR-based sequential sampling process for reliability analysis. The effectiveness of the proposed method is demonstrated using two mathematical and one practical case studies in Section 4. Section 5 gives several concluding remarks.

2 Review of Sequential Kriging-based Reliability Analysis

As mentioned in the introduction, one desirable property that the kriging model possesses is its ability to provide a probabilistic estimation. This property offers great benefits to sequential kriging-based reliability analysis. Subsection 2.1 briefly introduces the fundamentals of the kriging model, and Subsection 2.2 reviews four representative acquisition functions for sequential kriging-based reliability analysis and compares them in terms of their utility functions.

2.1 Kriging Model

A kriging model consists of two parts, a trend function $\mathbf{h}(\mathbf{x})\boldsymbol{\beta}$ and a Gaussian process $Z(\mathbf{x})$ [21], where $\mathbf{h}(\mathbf{x}) = [h_1, \ldots, h_p]^{\mathrm{T}}$ denotes p basis functions and $\boldsymbol{\beta}$ denotes the corresponding coefficients. In sequential kriging-based reliability analysis, the kriging model of a performance function $G(\mathbf{x})$ can be expressed as

$$\hat{G}(\mathbf{x}) = \mathbf{h}(\mathbf{x})\boldsymbol{\beta} + Z(\mathbf{x}) \tag{2}$$

where $Z(\mathbf{x})$ is a Gaussian process defined by zero mean, variance s^2, and correlation matrix Ψ. For a kriging model constructed with a sample data-set $D_t = \{(\mathbf{x}_1, y_1), \ldots, (\mathbf{x}_t, y_t)\}$, the correlation matrix Ψ takes the following form:

$$\Psi = \begin{pmatrix} \psi(\mathbf{x}_1, \mathbf{x}_1) & \cdots & \psi(\mathbf{x}_1, \mathbf{x}_t) \\ \vdots & \vdots & \vdots \\ \psi(\mathbf{x}_t, \mathbf{x}_1) & \cdots & \psi(\mathbf{x}_t, \mathbf{x}_t) \end{pmatrix} \tag{3}$$

where each entry $\psi(.,.)$ in the correlation matrix denotes a kernel function. The kernel function is defined in such a way that the points closer to each other take higher function values. This study employs a squared exponential kernel function in the kriging model with hyper-parameters $\boldsymbol{\theta}$:

$$\psi(\mathbf{x}_i, \mathbf{x}_j) = \exp\left(-\frac{1}{2} (\mathbf{x}_i - \mathbf{x}_j)^T \operatorname{diag}(\boldsymbol{\theta})^{-2} (\mathbf{x}_i - \mathbf{x}_j) \right) \tag{4}$$

where $\operatorname{diag}(\boldsymbol{\theta})$ denotes a vector with d elements corresponding to the d dimensions of $\mathbf{x}$. The values of the hyper-parameters $\boldsymbol{\theta}$ is crucial as these values affect the smoothness of the predictions. Usually, these values are estimated by maximizing the likelihood of the observations. After estimating $\boldsymbol{\theta}$, the prediction of the performance function at a new point $\mathbf{x}$ (with an unknown performance output) takes a Gaussian distribution form, $\hat{G}(\mathbf{x}) \equiv N\left(\hat{G} \middle| \mu_{\hat{G}}, \sigma_{\hat{G}}\right)$, where the mean $\mu_{\hat{G}}$ and standard deviation $\sigma_{\hat{G}}$ are determined as [21]

$$\mu_{\hat{G}}(\mathbf{x}) = \mathbf{h}(\mathbf{x})\boldsymbol{\beta} + \mathbf{r}(\mathbf{x}) \cdot \Psi^{-1} \cdot (\mathbf{y} - \mathbf{F}\boldsymbol{\beta}) \tag{5}$$

$$\sigma_{\hat{G}}^2(\mathbf{x}) = s^2 \left[1 - \mathbf{r}(\mathbf{x}) \Psi^{-1} \mathbf{r}(\mathbf{x})^{\mathrm{T}} + \frac{\left(1 - \mathbf{F}^{\mathrm{T}} \Psi^{-1} \mathbf{r}(\mathbf{x})^{\mathrm{T}}\right)}{\mathbf{F}^{\mathrm{T}} \Psi^{-1} \mathbf{F}} \right] \tag{6}$$

where $\mathbf{y} = [y_1, \ldots, y_t]^{\mathrm{T}}$ denotes a vector consisting of t responses, $\mathbf{F}$ denotes a $t \times p$ matrix with the i^{th} row being $\mathbf{h}(\mathbf{x}_i)^{\mathrm{T}}$ $(1 \le i \le t)$, and $r(\mathbf{x}) = [\psi(\mathbf{x}, \mathbf{x}_1), \ldots, \psi(\mathbf{x}, \mathbf{x}_t)]^{\mathrm{T}}$ denotes a correlation vector. Further details on the kriging model can be found in Ref. [25].

2.2 Sequential Kriging-Based Reliability Analysis

2.2.1 Expected Feasibility Function

In sequential kriging-based reliability analysis, a high accuracy in the approximation of LSF, which separates the safety and failure regions, leads to a high accuracy in reliability estimation. Based on this principle, the EFF [15] is introduced to indicate how well the performance function value at a candidate sample point (e.g., a random point generated using MCS) is expected to satisfy the limit state, G=0. This expectation can be calculated by integrating the feasibility function (i.e., $\tau - \left|\hat{G}\right|$) over a critical range $[-\tau, \tau]$:

$$\mathrm{EFF}(\mathbf{x}) = \mathbb{E}\left[\left(\tau - \left| \hat{G}(\mathbf{x}) \right| \right) \cdot \mathrm{H}\left(\tau - \left| \hat{G}(\mathbf{x}) \right| \right) \right] = \int_{-\tau}^{+\tau} \left(\tau - \left| \hat{G} \right| \right) f_{\hat{G}} \, d\hat{G} \tag{7}$$

where $f_{\hat{G}}$ denotes PDF of the kriging posterior $\hat{G}(\mathbf{x})$, $\hat{G}$ denotes a random realization of $\hat{G}(\mathbf{x})$, τ denotes the threshold parameter that is often set to be proportional to the standard deviation of the kriging posterior (e.g., $2\sigma_{\hat{G}}(\mathbf{x})$), and H(·) denotes the standard Heaviside step function. EFF favors the candidate sample points where the predicted performance function values are close to zero and/or the prediction uncertainty is high.

In decision analysis, a utility function quantifies the effectiveness of a strategy or policy [26]. As for the acquisition function in sequential sampling, the utility function at a candidate sample point should be defined in a way that reflects the effectiveness of adding this sample to the existing sample data set [27]. Under the context of sequential kriging-based reliability analysis, we identify an optimal sample by maximizing the expected utility in the presence of the uncertainty in the kriging posterior. Mathematically, the expected utility can be expressed as

$$\mathrm{EU}(\mathbf{x}) = \int_{-\infty}^{+\infty} u(\hat{G}) f_{\hat{G}} \, d\hat{G} \tag{8}$$

where $u\left(\hat{G}\right)$ denotes the utility function as a function of $\hat{G}$. Eq. (8) provides a generic expression of an acquisition function in terms of its utility function. By comparing the definition of EFF in Eq. (7) and that of EU in Eq. (8), the utility function of EFF takes the following form:

$$u(\hat{G}) = \begin{cases} \tau - |\hat{G}| & \text{if } |\hat{G}| < \tau \\ 0 & \text{otherwise} \end{cases} \tag{9}$$

2.2.2 Maximum Confidence Enhancement

The reliability estimation accuracy of a kriging model is determined by its accuracy in predicting the signs of the performance function values at the candidate sample points. A candidate sample point $\mathbf{x}$ is either classified into the failure region ($\mu_{\hat{G}}(\mathbf{x}) > 0$) or safety region ($\mu_{\hat{G}}(\mathbf{x}) \leq 0$) based on the sign of the kriging prediction $\mu_{\hat{G}}(\mathbf{x})$. To this end, another well-known acquisition function named MCE [16] is defined by considering the probability that the kriging model correctly predicts the sign of the performance function value at a candidate sample point. In MCE, the confidence level (CL) for correctly predicting the sign is defined as

$$\mathrm{CL}(\mathbf{x}) = P\left(\hat{G}(\mathbf{x}) \cdot \frac{\mu_{\hat{G}}(\mathbf{x})}{|\mu_{\hat{G}}(\mathbf{x})|} \geq 0 \right) = \Phi\left(\frac{|\mu_{\hat{G}}(\mathbf{x})|}{\sigma_{\hat{G}}(\mathbf{x})} \right) \tag{10}$$

$\mathrm{CL}(\cdot)$ is a positive value within [0.5, 1]. Based on the defined CL, MCE is defined as

$$\mathrm{MCE}(\mathbf{x}) = (1 - \mathrm{CL}(\mathbf{x})) \cdot f_{\mathbf{x}}(\mathbf{x}) \cdot \sqrt{\sigma_{\hat{G}}(\mathbf{x})} \tag{11}$$

where $f_{\mathbf{x}}(\mathbf{x})$ denotes the PDF of a candidate sample point $\mathbf{x}$, the multiplication of $(1 - \mathrm{CL}(\mathbf{x}))$ and $f_{\mathbf{x}}(\mathbf{x})$ favors points that are close to the LSF and have higher PDF values, and $\sqrt{\sigma_{\hat{G}}(\mathbf{x})}$ favors points with high prediction uncertainty. By comparing Eq. (10) with Eq. (8), the CL in MCE can be expressed with the following utility function:

$$u(\hat{G}) = \begin{cases} 1 & \text{if } \hat{G} \cdot \mu_{\hat{G}}(\mathbf{x}) < 0 \\ 0 & \text{otherwise} \end{cases} \tag{12}$$

2.2.3 Expected Risk Function

As reviewed in Subsection 2.2.2, MCE is proposed based on the probability that the kriging model correctly predicts the sign of the performance function at a candidate sample point. Alternatively, the ERF [17] is proposed by quantifying the risk that a kriging model incorrectly identifies the sign. In ERF, a risk indicator (a function of $\hat{G}(\mathbf{x})$) is defined to quantify the extent that the value of $\hat{G}(\mathbf{x})$ is less than or equal to zero when $\mu_{\hat{G}}(\mathbf{x}) > 0$, and the extent that the value of $\hat{G}(\mathbf{x})$ is greater than zero when $\mu_{\hat{G}}(\mathbf{x}) \leq 0$, expressed as

$$\mathrm{RI}(\hat{G}(\mathbf{x})) = \begin{cases} \max[(0 - \hat{G}(\mathbf{x})), 0] & \text{if } \mu_{\hat{G}}(\mathbf{x}) > 0 \\ \max[(\hat{G}(\mathbf{x}) - 0), 0] & \text{if } \mu_{\hat{G}}(\mathbf{x}) \leq 0 \end{cases} \tag{13}$$

ERF is then defined as the expected value of the risk indicator, expressed as

$$\mathrm{ERF}(\mathbf{x}) = \mathbb{E}[\mathrm{RI}(\hat{G}(\mathbf{x}))] = \int_0^{\infty} -\mathrm{sign}\left[\mu_{\hat{G}}(\mathbf{x}) \right] \hat{G} f_{\hat{G}}\, d\hat{G} \tag{14}$$

where $\mathrm{sign}(\cdot)$ denotes the sign function. The utility function of ERF can be expressed as

$$u(\hat{G}) = \begin{cases} \hat{G} & \text{if } \hat{G} \cdot \mu_{\hat{G}}(\mathbf{x}) < 0 \\ 0 & \text{otherwise} \end{cases} \tag{15}$$

2.2.4 Sequential Exploration-Exploitation with Dynamic Trade-off

All the aforementioned three acquisition functions assign fixed weights on exploitation (regions close to the LSF) and exploration (regions with high prediction uncertainty). To enable dynamic adjustment of the weights, Sadoughi et al. [21] proposed an acquisition function called SEEDT, expressed as

$$\mathrm{SEEDT}(\mathbf{x}) = f_{\mathbf{x}}(\mathbf{x}) \cdot \frac{\alpha_t^{\,2}\, \sigma_{\hat{G}}(\mathbf{x})}{\sqrt{1 + \alpha_t^{\,2}}} e^{-\frac{\mu_{\hat{G}}(\mathbf{x})^2}{2\sigma_{\hat{G}}(\mathbf{x})\sqrt{1+\alpha_t^{\,2}}}} \tag{16}$$

where α_t denotes an exploration-exploitation trade-off coefficient that measures the uncertainty in LSF prediction, whose value decreases as the kriging model achieves more accurate prediction. With the assistance of α_t, SEEDT

possesses the capability to dynamically control the exploration-exploitation trade-off. Besides, a Gaussian decay function is defined as the utility function of SEEDT, which takes the following form

$$u\left(\hat{G}\right) = \sigma' \cdot \exp\left[\frac{-\hat{G}^2}{2\sigma'^2}\right] \tag{17}$$

where $\sigma' = \alpha_t \cdot \sigma_{\hat{G}}(\mathbf{x})$, which is defined as an intermediate variable to simplify the expression form of $u\left(\hat{G}\right)$. From Eq. (17), the utility function of SEEDT is a smooth and continuous function.

2.2.5 Comparison of the Utility Functions in Different Acquisition Functions

The utility functions of the four acquisition functions are graphically compared in Fig. 1. As can be observed from this figure, the utility function of MCE takes the shape of the Heaviside step function (Fig. 1 (b)), while those of EFF and ERF take triangle shapes (Fig. 1 (a) and (c)). With a constant utility function, MCE only considers the probability of improvement without the magnitude of $\hat{G}$ (i.e., different $\hat{G}$ values are weighed equally), and covers a partial range of $\hat{G}$ (i.e., $\hat{G} \cdot \mu_{\hat{G}}(\mathbf{x}) > 0$). EFF and ERF consider the magnitude of $\hat{G}$ in their triangle shape utility functions. However, EFF only covers a narrow range of $\hat{G}$ (i.e., $[-\tau, \tau]$) and ERF only covers a partial range defined by $\hat{G} \cdot \mu_{\hat{G}}(\mathbf{x}) < 0$. On the other hand, the utility function of SEEDT takes the Gaussian decay function form (Fig. 1 (d)), which is continuous and smooth over all ranges of $\hat{G}$.

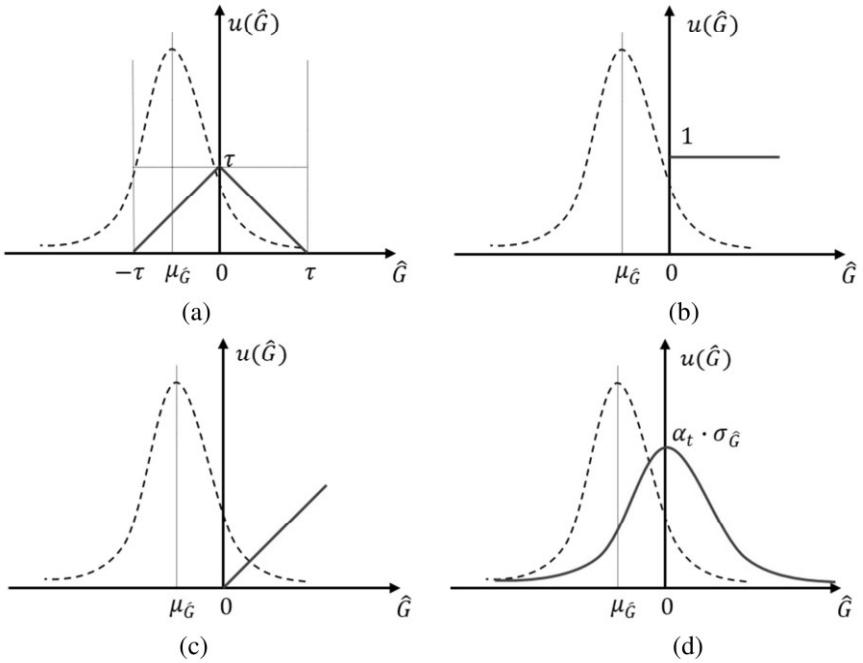

Fig. 1 Comparison of the utility functions in EFF (a), MCE (b), ERF (c), and SEEDT (d).

The differences in the utility functions of the four acquisition functions result in different weights assigned to exploration and exploitation during the sequential sampling process. However, the optimal weights at a certain stage of the sequential sampling process or the optimal acquisition function for a specific problem is usually unknown to us. To make full use of different acquisition functions in the sequential sampling process, this study leverages a portfolio to include multiple acquisition functions and suggest multiple optimal samples at each iteration. Then, a meta-criterion is defined to select the best sample among the optimal samples.

3 Methodology

This section first introduces the uncertainty indicator of the LSF prediction, which indirectly indicates the accuracy of the kriging model in the LSF prediction. Then, a meta-criterion, EUR, is introduced to select the best sample among the optimal samples suggested by the acquisition functions in the portfolio. Finally, the overall procedure of the EUR-based sequential sampling process is summarized.

3.1 Uncertainty Indicator of the LSF Prediction

LSF divides the input (**x**) space into the safety region and the failure region. In this study, we define an uncertainty indicator η_t to quantify the uncertainty in the LSF prediction and indirectly measure the accuracy of the kriging model in the LSF prediction.

The kriging model provides not only the mean prediction of the performance function at a candidate sample point $\mu_{\hat{G}}(\mathbf{x})$ but also the uncertainty of the prediction $\sigma_{\hat{G}}(\mathbf{x})$. Based on these two quantities, we can define the $100\left(1-\frac{\gamma}{2}\right)\%$ confidence interval of the prediction at a candidate sample point with significance level γ, expressed as $CI_\gamma(\mathbf{x}) = [\mu_{\hat{G}}(\mathbf{x}) - z_{\gamma/2}\sigma_{\hat{G}}(\mathbf{x}), \mu_{\hat{G}}(\mathbf{x}) + z_{\gamma/2}\sigma_{\hat{G}}(\mathbf{x})]$. Depending on whether the value zero falls into this interval, the probable LSF region in the input (**x**) space can be identified as $\Omega^{LSF} = \{\mathbf{x} \mid 0 \in CI_\gamma(\mathbf{x})\}$. Ω^{LSF} is expected to cover a large region in the input space when the prediction uncertainty is high and a small region when the prediction uncertainty is low. Inspired by this expectation, we use the probability that a candidate sample point **x** falls into Ω^{LSF} to quantify the uncertainty of the LSF prediction and indirectly indicate the accuracy of the kriging model. This probability is defined as the uncertainty indicator η_t, expressed as

$$\eta_t = P\left(\mathbf{x} \in \Omega^{LSF}\right) = \int_{\mathbf{x}\in\Omega^{LSF}} f_{\mathbf{x}}(\mathbf{x})\, d\mathbf{x} \tag{18}$$

Since the integration does not have an analytical solution, η_t is approximated as the fraction of the candidate sample points that fall into Ω^{LSF}, expressed as

$$\eta_t \approx \frac{1}{n_{MCS}} \sum_{i=1}^{n_{MCS}} I_{\Omega^{LSF},P}(\mathbf{x}_i); \quad I_{\Omega^{LSF}}(\mathbf{x}_i) = \begin{cases} 1 & \mathbf{x}_i \in \Omega^{LSF} \\ 0 & \text{otherwise} \end{cases} \tag{19}$$

Figure 2 illustrates the definition of the probable LSF region Ω^{LSF} and the uncertainty indicator η_t. The shaded area in the vicinity of the mean predicted LSF (red dash line) denotes the probable LSF region Ω^{LSF}. The red squares and green circles show the candidate sample points that are located outside and inside Ω^{LSF}, respectively. Then, η_t can be approximated using Eq. (19). In general, η_t exhibits a decreasing trend over the sequential sampling process.

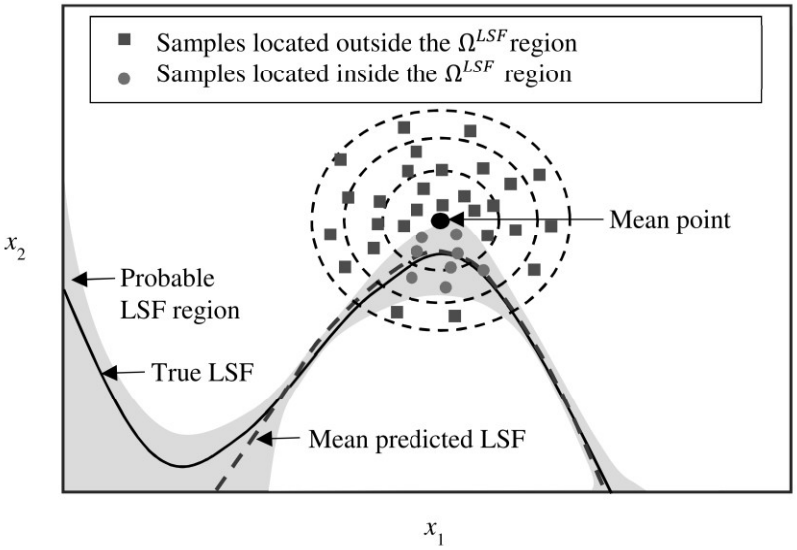

Fig. 2 Illustration of the probable LSF region Ω^{LSF} and the uncertainty indicator η_t

3.2 EUR

Based on the uncertainty indicator η_t defined in Subsection 3.1, we propose a meta-criterion called EUR to quantify the expected uncertainty reduction of the LSF prediction by adding the optimal sample point suggested by an acquisition function. This proposed meta-criterion allows choosing the sample point that is expected to bring the highest uncertainty reduction at each iteration of the sequential sampling process.

EUR is defined as follows. Let η_{t+1} denote the uncertainty indicator after the next sample point $\{(\mathbf{x}_{t+1}, y_{t+1})\}$ is added to the existing sample data set D_t. The uncertainty change in the LSF prediction can be calculated as $\Delta\eta_{t+1} = \eta_t - \eta_{t+1}$, which is expected to be greater than zero since the uncertainty of the LSF prediction is expected to decrease. It should be noted that the value of y_{t+1} is unavailable before we evaluate the true performance function at $\mathbf{x}_{t+1}$, but the posterior distribution $p(y_{t+1}|D_t, \mathbf{x}_{t+1})$ can be predicted by the kriging model that is constructed with the existing sample data set D_t. Based on the posterior distribution $p(y_{t+1}|D_t, \mathbf{x}_{t+1})$, EUR can be formulated as

$$\mathrm{EUR}(\mathbf{x}_{t+1} \mid D_t) = \mathbb{E}_{p(y_{t+1}|D_t, \mathbf{x}_{t+1})}[\Delta\eta_{t+1}(y_{t+1}) \mid D_t \cup \{(\mathbf{x}_{t+1}, y_{t+1})\}] = \int \Delta\eta_{t+1}(y_{t+1}) p(y_{t+1} \mid D_t, \mathbf{x}_{t+1}) dy_{t+1} \quad (20)$$

The integration in Eq. (20) does not have an analytical solution. As an alternative, it can be approximated with MCS by sampling from $p(y_{t+1}|D_t, \mathbf{x}_{t+1})$:

$$\mathrm{EUR}(\mathbf{x}_{t+1} \mid D_t) \approx \frac{1}{N} \sum_{n=1}^{N} \Delta\eta_{t+1}(y_{t+1}^{(n)} \mid \widetilde{D}_{t+1}^{(n)}) \quad (21)$$

where $y_{t+1}^{(n)}$ denotes the n^{th} hallucinated point sampled from the posterior distribution $p(y_{t+1}|D_t, \mathbf{x}_{t+1})$, $\widetilde{D}_{t+1}^{(n)}$ denotes the hallucinated sample data set after $\{(\mathbf{x}_{t+1}, y_{t+1}^{(n)})\}$ is added to D_t, i.e., $\widetilde{D}_{t+1}^{(n)} = D_t \cup \{(\mathbf{x}_{t+1}, y_{t+1}^{(n)})\}$, and N denotes the total number of hallucinated points (N = 1,000 in this study). To reduce the variance of this approximation, the same random seed is used to sample the hallucinated points from the posterior distributions at each iteration. The sample point $\mathbf{x}_{t+1}^{*}$ that maximizes EUR is added to the existing sample data set D_t to update the kriging model:

$$\mathbf{x}_{t+1}^{*} = \arg\max \mathrm{EUR}(\mathbf{x}_{t+1} \mid D_t) \quad (22)$$

The procedure of calculating EUR is given in Table 1 and a visualization of the key steps is shown in Fig. 3.

Table 1 Procedure of calculating EUR

Algorithm 1: EUR

Input: optimal sample $\{\mathbf{x}_{t+1}\}$, sample data set D_t

1 Calculate the uncertainty indicator η_t at the current iteration t
2 Generate N hallucinated points $y_{t+1}^{(n)}$ (n=1,2…N) based on $p(y_{t+1}|D_t, \mathbf{x}_{t+1})$
3 **for** $n = 1 : N$ **do**
4 Augment the sample data set with the nth hallucinated point
$$\widetilde{D}_{t+1}^{(n)} = D^t \cup \{(\mathbf{x}_{t+1}, y_{t+1}^{(n)})\}$$
5 Update the kriging model based on $\widetilde{D}_{t+1}^{(n)}$
6 Calculate the uncertainty indictor $\eta_{t+1}^{(n)}$ of the updated kriging model
7 Calculate the uncertainty reduction $\Delta\eta_{t+1}^{(n)} = \eta_t - \eta_{t+1}^{(n)}$
8 **end for**
9 $\mathrm{EUR}(\mathbf{x}_{t+1}|D_t) \approx \frac{1}{N}\sum_{n=1}^{N} \Delta\eta_{t+1}^{(n)}$

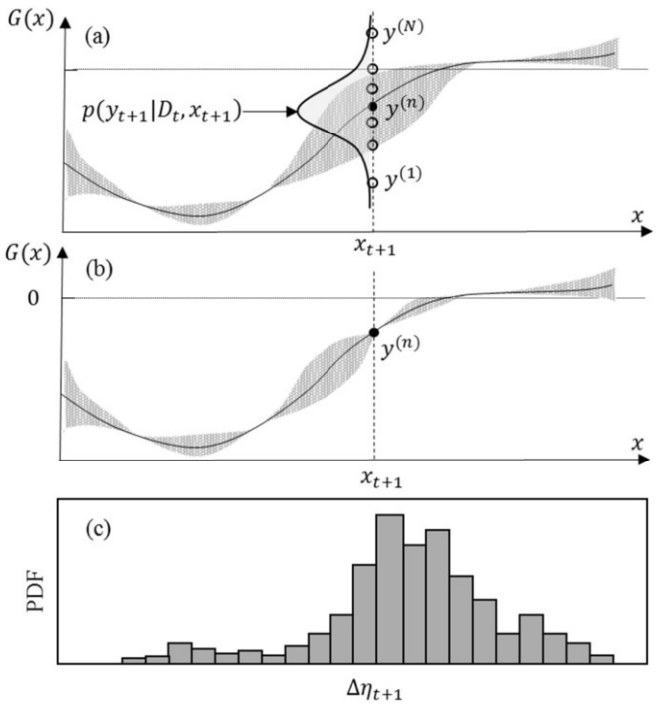

Fig. 3 A visualization of the key steps in calculating EUR: (a) generate N hallucinated points $y_{t+1}^{(n)}$ from $p(y_{t+1}|D_t, \mathbf{x}_{t+1})$, (b) update the kriging model based on $\widetilde{D}_{t+1}^{(n)}$, and (c) calculate the uncertainty reduction $\Delta\eta_{t+1}^{(n)} = \eta_t - \eta_{t+1}^{(n)}$ for each hallucinated point and draw an empirical PDF.

3.3 EUR-based Sequential Sampling Process for Reliability Analysis

It is difficult to find an acquisition function that outperforms others on all problem cases. Further, the best-performing acquisition function may change at various stages of the sequential sampling process. To make full use of different acquisition functions, EUR is employed as the meta-criterion to select the best sample among the optimal samples suggested by the acquisition functions in a portfolio. As EUR is calculated for each optimal sample point, the point that maximizes EUR is expected to result in the highest uncertainty reduction of the LSF prediction. It should be mentioned that EUR could be directly used as an acquisition function to select the best sample point among all the candidate sample points (e.g., $n_{MCS} = 10^7$). However, the computational cost will be extremely high given that N kriging models (N = 1,000 in this study) need to be constructed over each candidate point to calculate the EUR value. Thus, we restrict the candidate points for EUR evaluation to be the optimal samples that are suggested by the acquisition functions in the portfolio.

The procedure of using EUR for reliability analysis is elaborated in Table 2. Let $\{ACQ_k\}_{k=1}^K$ denote K acquisition functions and t denote the current iteration. First, K optimal samples are identified by maximizing the K acquisition functions (line 5), which are denoted as $\{\mathbf{x}_{t+1}^{*,k}\}_{k=1}^K$. Then, the EUR values for the K optimal samples are calculated and the sample point $\mathbf{x}_{t+1}^*$ that gives the highest EUR value will be selected as the best sample point. Finally, the performance function is evaluated at $\mathbf{x}_{t+1}^*$, and this sample point is added to the existing sample data set D_t (lines 8-11). This procedure is repeated until the target accuracy (see the convergence estimator (CE) in line 12) is achieved or the predefined number of samples is reached. Further details on the convergence estimator can be found in Ref. [18].

Table 2 Procedure of calculating EUR for reliability analysis

Algorithm 2: Reliability Analysis Using EUR

Build the initial kriging model $\hat{G}(\mathbf{x})$ based on the initial data set D_0
$t = 0$
while $t < T$ & $CE > CE_0$ **do**
  for $k = 1 : K$ **do**
    Suggest a new optimal sample point $\mathbf{x}_{t+1}^{*,k}$ that maximizes ACQ_k:
$$\mathbf{x}_{t+1}^{*,k} = \arg\max_{\mathbf{x}} ACQ_k(\mathbf{x}|D_t)$$
    Calculate EUR($\mathbf{x}_{t+1}^{*,k}|D_t$) based on **Algorithm 1**
  end for
  Select the best sample point $\mathbf{x}_{t+1}^{*}$ that maximizes EUR:
$$\mathbf{x}_{t+1}^{*} = \arg\max_{1\le k\le K} \mathrm{EUR}(\mathbf{x}_{t+1}^{*,k}|D_t)$$
  Observe the performance function value at $\mathbf{x}_{t+1}^{*}$:
$$y_{t+1} = G(\mathbf{x}_{t+1}^{*})$$
  Augment the existing data set D_t with the new sample point:
$$D_{t+1} = D_t \cup \{(\mathbf{x}_{t+1}^{*}, y_{t+1})\}$$
  Update the kriging model $\hat{G}(\mathbf{x})$ based on the data set D_{t+1}
  Evaluate the convergence estimator
$$\mathrm{CE} = \int_{|\hat{G}(\mathbf{x})|<\sigma(\mathbf{x}))} f_{\mathbf{x}}(\mathbf{x})d\mathbf{x}$$
  $t = t + 1$
end while
Perform MCS on $\hat{G}(\mathbf{x})$ for reliability estimation

4 Case Studies

In this section, we employ two mathematical and one practical case studies to evaluate the performance of the proposed method. The reliability estimation accuracy of the EUR-based sequential sampling process (or the EUR-based method) is compared with that of the method with the single use of each acquisition function. Case study 1 is designed to compare the performance of different methods at different nonlinearity levels of the performance function. Case study 2 employs a highly nonlinear performance function with strong variate interactions to investigate the effects of different reliability levels on the performance of different methods in reliability analysis. Finally, case study 3 is used to evaluate the practicality of the proposed method using a real-world engineering problem.

The reliability estimation results by direct MCS (i.e., R_{MCS}) are employed as the benchmark reliability levels in each case study. The reliability error is then defined as the difference between the reliability estimate by each method and the benchmark reliability level (i.e., $\varepsilon = \hat{R} - R_{MCS}$). This error is employed to evaluate the performance of each method in reliability analysis. Due to the randomness in generating the initial samples with LHS and random MCS points, the reliability errors estimated by different methods contain uncertainties. To capture the uncertainties, we repeatedly run each method 20 times in each problem case. The performance of each method is then presented as the mean and standard deviation ($\mu_\varepsilon \pm \sigma_\varepsilon$) of the reliability error over the 20 repeated runs.

4.1 Case Study 1: A 2D Example with High Nonlinearity

The first case study has a highly nonlinear performance function, which consists of a polynomial part, a trigonometric part, and a constant [15]. The performance function is defined as

$$G(\mathbf{x}) = \frac{(x_1^2 + 4)(x_2 - 1)}{20} - \cos\left(\frac{ax_1}{2}\right) - 1.5 \tag{23}$$

where the coefficient a is used to adjust the nonlinearity of $G(\mathbf{x})$. The two input random variables x_1 and x_2 are considered to be independent from each other, both of which follow the normal distribution (μ=1.5, σ=1).

We first verify the effectiveness of EUR in quantifying the uncertainty reduction of the LSF prediction (Eq. (21)) for the case a=9. In this verification, we track the simulated values of uncertainty reduction at each iteration of sequential sampling and compare them with the true uncertainty reduction. Fig. 4 (a) shows the comparison results (the error bar denotes the expected uncertainty reduction and its 95% confidence interval). We can observe that the simulation produces a reasonably accurate approximation of the uncertainty reduction at each iteration, although slightly higher approximation errors are observed during the first few iterations than those in the later iterations. Figs. 4 (b), (c), and (d) show the three sets of MCS candidates (the green solid circles) located inside Ω^{LSF} at iterations 8, 9, and 10, respectively. These sets of candidate points are used to approximate the uncertainty indicators at the three iterations (Eq. (19)). The results in Fig. 4 show that (1) the accuracy in the LSF prediction generally increases as more samples are included in the kriging model, and (2) such accuracy improvement goes along with the reduction of uncertainty in the LSF prediction.

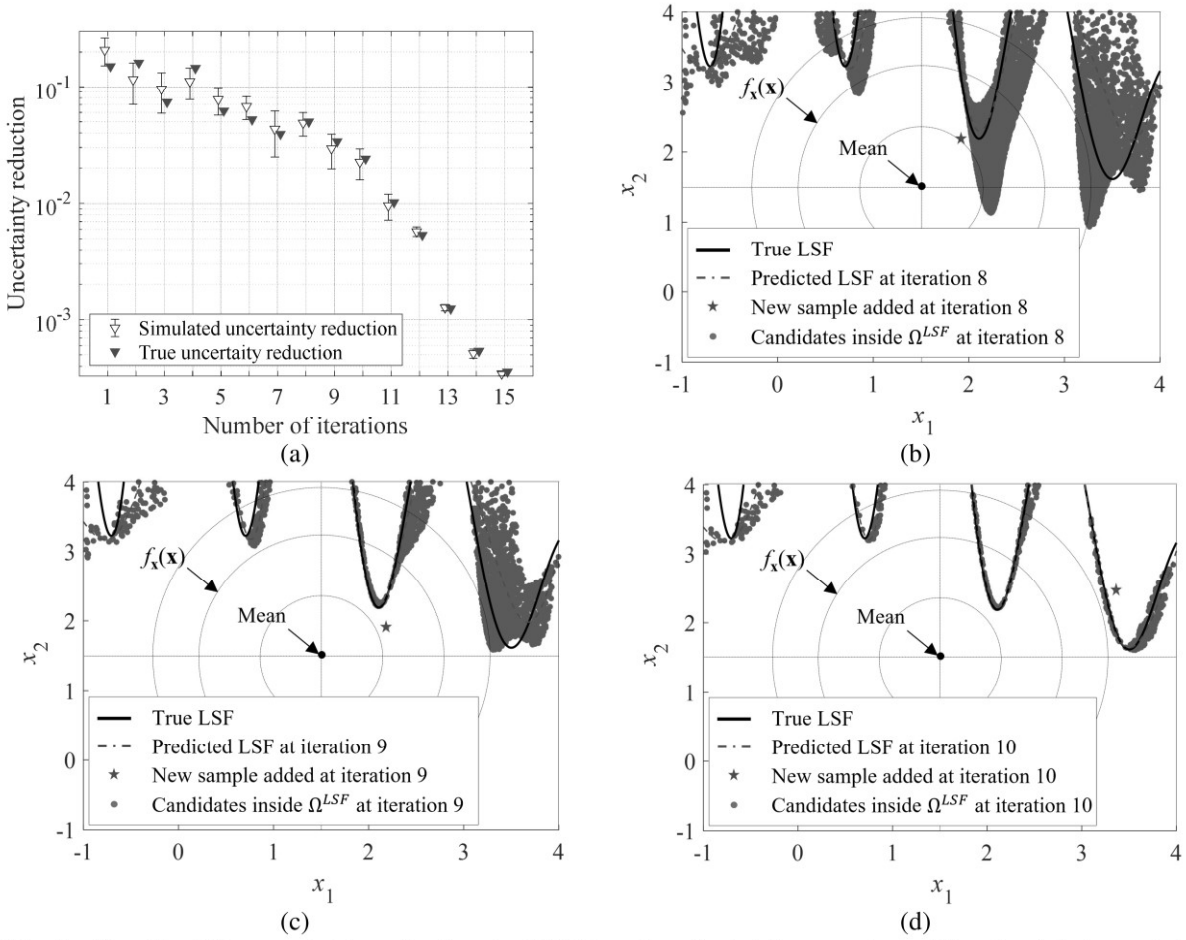

Fig. 4 Results of the uncertainty reductions by EUR-based method: (a) comparison of the simulated uncertainty reduction and true uncertainty reduction at each iteration, (b-d) MCS candidates located inside Ω^{LSF} at iterations 8, 9, and 10.

We then compare different methods in terms of reliability estimation and uncertainty reduction. Fig. 5 presents the comparison results for the case a=9. Fig. 5 (a) and 5 (b) show the evolutions of the absolute reliability errors (i.e., $|\varepsilon|$) and the uncertainty indicator η_t over iterations, respectively. Fig. 5 (c) shows a snapshot of the probability distributions of uncertainty reduction ($\Delta\eta_t$) for the four acquisition functions, taken at iteration 6 of sequential sampling. Fig. 5 (d) shows the selected acquisition function for each iteration during one run of the sequential sampling process of EUR-based method. It can be observed from Fig. 5 that (1) the average absolute reliability errors of EUR-based method are the lowest among all the methods, and (2) the best-performing acquisition function changes at different iterations of the sequential sampling process.

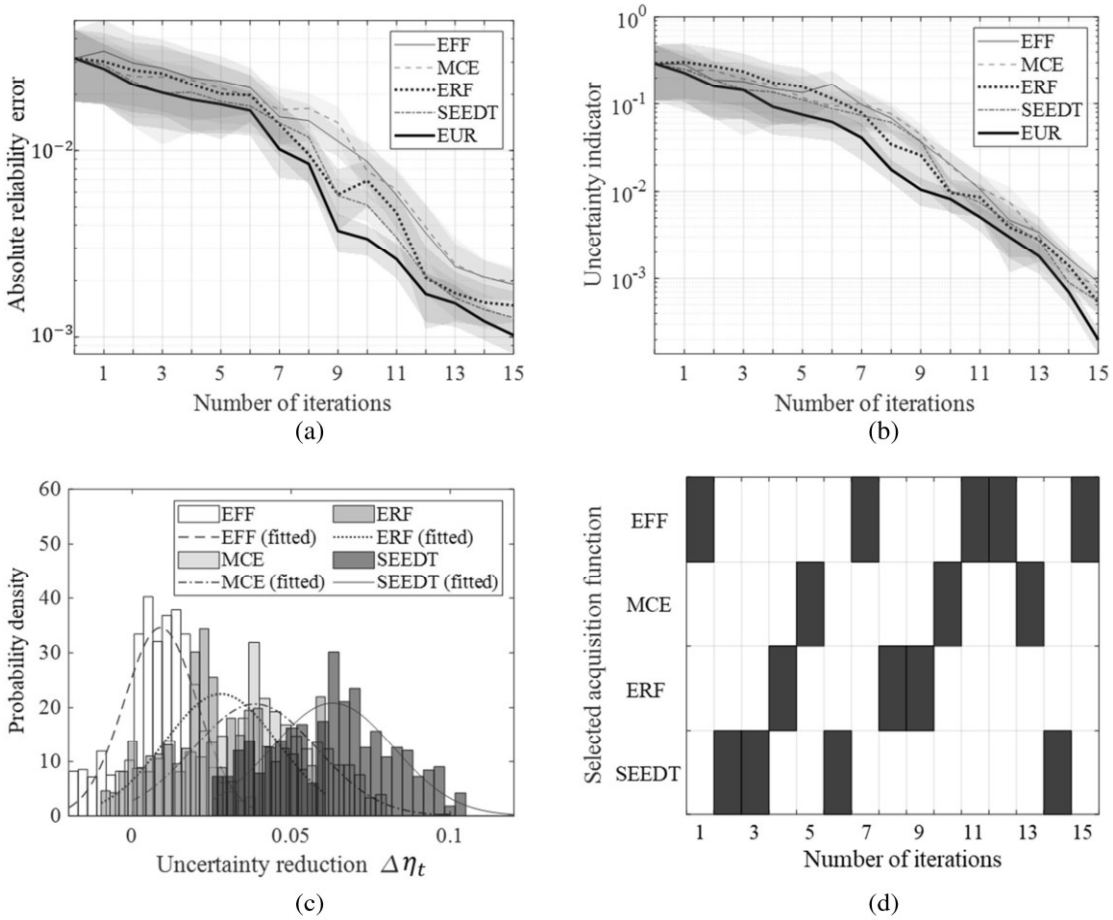

Fig. 5 Results of different methods for a=9: (a) evolution of the absolute reliability error, (b) evolution of the uncertainty indicator η_t, (c) a snapshot of the probability distributions of uncertainty reduction for the four acquisition functions at iteration # of sequential sampling, and (d) a snapshot of the selected acquisition function for each iteration.

Table 3 summarizes the numbers of function evaluations (FEs), benchmark reliability estimates with MCS (n_{MCS} = 10^7), and reliability errors of the five methods. From the results, we can observe that the EUR-based method outperforms the single use of any constituent acquisition function in the portfolio. While the improvement is not significant over the best-performing acquisition functions for different nonlinearity levels of the performance function, this is still desirable considering that the best-performing acquisition functions change for different problem cases and no prior information about the best-performing acquisition function is available.

Table 3 Reliability estimation results of different methods

Method		a=3	a=5	a=7	a=9
EFF	$\mu_\varepsilon \pm \sigma_\varepsilon$	-0.000925±0.000583	0.001313±0.000613	0.003317±0.002662	0.001971±0.001131
	No. of FEs	25 (10 LHS samples + 15 sequential samples)			
MCE	$\mu_\varepsilon \pm \sigma_\varepsilon$	-0.000631±0.000491	0.001936±0.000715	0.002046±0.001709	0.001907±0.001083
	No. of FEs	25 (10 LHS samples + 15 sequential samples)			
ERF	$\mu_\varepsilon \pm \sigma_\varepsilon$	-0.000837±0.000562	0.000821±0.000529	0.001729±0.001045	0.001475±0.001290
	No. of FEs	25 (10 LHS samples + 15 sequential samples)			
SEEDT	$\mu_\varepsilon \pm \sigma_\varepsilon$	-0.000516±0.000406	0.001403±0.000689	0.002112±0.001597	0.001267±0.000829
	No. of FEs	25 (10 LHS samples + 15 sequential samples)			
EUR	$\mu_\varepsilon \pm \sigma_\varepsilon$	-0.000479±0.000324	0.000732±0.000541	0.001612±0.001133	0.001022±0.000593
	No. of FEs	25 (10 LHS samples + 15 sequential samples)			
MCS	$\mu_{R_{MCS}} \pm \sigma_{R_{MCS}}$	0.928326±0.000441	0.970168±0.000327	0.960677±0.000288	0.961216±0.000302
	No. of FEs	10,000,000			

4.2 Case Study 2: An 8D Example with Strong Variate Interactions

The second case study considers a two-degree-of-freedom primary-secondary system with uncertain damped oscillators in the presence of white noise [28]. The reliability level of the system varies depending on the load F_s. This problem has been investigated by many researchers due to its high nonlinearity and strong variate interactions [29,30]. The performance function of this system is mathematically expressed as

$$G(\mathbf{x}) = 3k_s\left(\frac{\pi S_0}{4\xi_s\omega_s^3}\left[\frac{\xi_a\xi_s}{\xi_p\xi_s(4\xi_a^2+\theta^2)+\gamma\xi_a^2}\frac{\left(\xi_p\omega_p^3+\xi_s\omega_s^3\right)\omega_p}{4\xi_a\omega_a^4}\right]\right)^{1/2} - F_s \tag{24}$$

where $\omega_p = \sqrt{k_p/m_p}$, $\omega_s = \sqrt{k_s/m_s}$, $\omega_a = (\omega_p + \omega_s)/2$, $\xi_a = (\xi_p + \xi_s)/2$, $\gamma = m_s/m_p$ and $\theta = (\omega_p - \omega_s)/\omega_a$, $\mathbf{x} = [\omega_p, \omega_s, \omega_a, \xi_a, \gamma, \theta]$. Table 4 summarizes the statistical information of the input variables.

Table 4 Statistical properties of input random variables in case study 2

Variable	Distribution	Mean	Standard deviation
k_p	Lognormal	1	0.2
k_s	Lognormal	0.01	2e-3
m_p	Lognormal	1.5	0.15
m_s	Lognormal	0.01	1e-3
ξ_p	Lognormal	0.05	0.02
ξ_s	Lognormal	0.02	0.01
F_s	Lognormal	13.5-16	1.5
S_0	Lognormal	100	10

With the reliability levels estimated by MCS as the benchmarks, changing the mean values of F_s from 13.5 N to 16.0 N results in four different reliability levels between 0.9822 and 0.9977. Fig. 6 graphically compares the reliability errors of EFF, MCE, ERF, SEEDT, and EUR at the four reliability levels. Table 6 summarizes the numbers of FEs, benchmark reliability estimates by MCS ($n_{MCS} = 10^7$), and reliability errors of the five methods. As seen in the Fig. 6 and Table 6, although EUR-based method does not always achieve the best accuracy among all

the methods, its average reliability estimation errors are the lowest with the least uncertainty during the 20 repeated runs. This is desirable considering that the best-performing acquisition functions change for different problem cases.

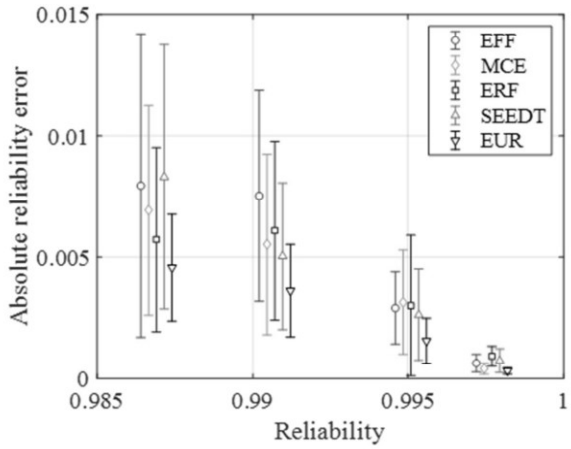

Fig. 6 Absolute reliability errors of different methods at different reliability levels

Table 5 Comparison of reliability estimation results for different methods

Method		F_s=13.5	F_s=14	F_s=15	F_s=16
EFF	$\mu_\varepsilon \pm \sigma_\varepsilon$	0.007952±0.006243	0.007531±0.004341	0.002916±0.001489	-0.000643±0.000367
	No. of FEs	80 (40 LHS samples + 40 sequential samples)			
MCE	$\mu_\varepsilon \pm \sigma_\varepsilon$	0.006933±0.004313	0.005531±0.003718	0.003152±0.002136	-0.000413±0.000231
	No. of FEs	80 (40 LHS samples + 40 sequential samples)			
ERF	$\mu_\varepsilon \pm \sigma_\varepsilon$	0.005725±0.003786	0.006093±0.003678	0.003012±0.002893	-0.000933±0.000413
	No. of FEs	80 (40 LHS samples + 40 sequential samples)			
SEEDT	$\mu_\varepsilon \pm \sigma_\varepsilon$	0.008312±0.005431	0.005041±0.003017	0.002634±0.001877	-0.000746±0.000494
	No. of FEs	80 (40 LHS samples + 40 sequential samples)			
EUR	$\mu_\varepsilon \pm \sigma_\varepsilon$	0.004571±0.002190	0.003622±0.001903	0.001563±0.000934	-0.000316±0.000129
	No. of FEs	80 (40 LHS samples + 40 sequential samples)			
MCS	$\mu_{R_{MCS}} \pm \sigma_{R_{MCS}}$	0.986932±0.000715	0.990692±0.000936	0.995112±0.000395	0.997786±0.000209
	No. of FEs	10,000,000			

4.3 Case Study 3: A Real-world Example

Passive friction dampers are widely used to mitigate vibrations in structural systems. Downey et al. [31] developed a cam-based passive variable friction damper (PVFD), which consists of two sliding friction plates. In this PVFD system, a normal force is applied to the sliding plates through a cam. A schematic of the PVFD system is shown in Fig. 7. As shown in the figure, a relative displacement between the two friction plates induces a rotation in the cam, which in turn causes a change in the normal friction force on the plates. By carefully designing the shape of the cam, a desired force-displacement behavior can be obtained for a specific vibration mitigation purpose. More details about the PVFD system can be found in [31].

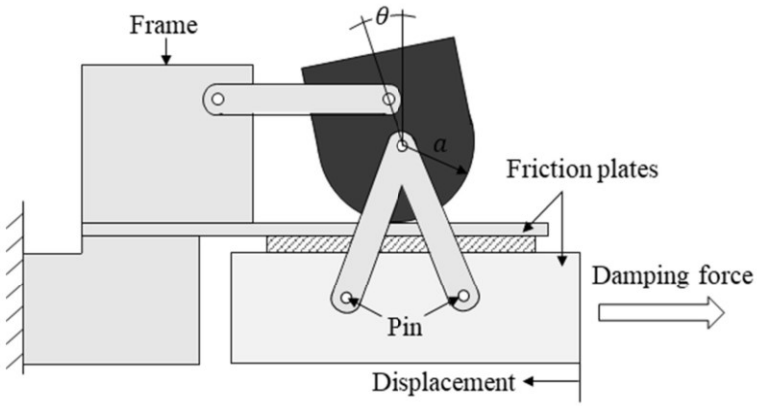

Fig. 7 Schematic of a PVFD system

A five-story building subjected to seismic loads is considered in this case study. Each story of the building is equipped with a PVFD system. Five elliptical cam shapes are selected for the PVFD systems, which have different semi-major axis lengths $a_i, i = 1,2, \ldots 5$. The distribution information of the five input random variables (i.e., $a_1 - a_5$) is summarized in Table 6. Semi-minor axis lengths and normal forces at $\theta = 0$ are 40mm and 700 N, respectively, for all the five cams. The PVFD system is modeled using the experimentally characterized LuGre model, whose friction force output is multiplied by a constant to obtain a realistic force for vibration mitigation of the building. Reliability analysis is performed on the five-story building equipped with PVFD systems under the setting in Table 6.

Table 6 Summary of the input random variables for the PVFD system example

Input random variable	Description	Dist. type	Mean	Std. dev.
$a_1(mm)$	Semi-major axis of cam 1	Normal	65.00	2.00
$a_2\ (mm)$	Semi-major axis of cam 2	Normal	71.00	2.00
$a_3(mm)$	Semi-major axis of cam 3	Normal	60.00	2.00
$a_4(mm)$	Semi-major axis of cam 4	Normal	67.00	2.00
$a_5(mm)$	Semi-major axis of cam 5	Normal	59.00	2.00

According to different safety requirement levels, the maximum displacement of the building D needs to be lower than the predefined displacement threshold D_0 as shown in Eq. (25). Then, the reliability of the PVFD system can be calculated as the probability that D is lower than D_0.

$$G(\mathbf{x}) = D(\mathbf{x}) - D_0 \tag{25}$$

Due to the significant computational cost of the true FEs (in evaluating the maximum displacement of the building), the direct MCS with 100,000 samples is performed according to the distributions of the input random variables. Then, the benchmark reliability levels under different displacement thresholds (i.e., $D_0 = 0.008$, 0.009, 0.01, and 0.011m) are calculated. Reliability analysis is then performed with different methods (i.e., EFF, MCE, ERF, SEEDT, and EUR). To reduce the randomness of the results, the same random seeds are used to generate the MCS random samples for each method (no uncertainty is involved in the progress of MCS). The reliability estimation results for different displacement thresholds are graphically compared in Fig. 8. Table 7 summarizes the number of FEs, benchmark reliability estimates by MCS, and reliability errors by the five methods. It can be observed that the EUR-based method outperforms the single use of any constituent acquisition function in the portfolio, while the best-performing acquisition functions change for different problems. The reliability estimation results of this real-world case study further verify that the proposed EUR-based method is effective in reliability analysis of engineered systems.